# Supplemental Data

# "Preclinical $^{89}$Zr-immunoPET of High Grade Serous Ovarian Cancer and Lymph Node Metastasis"

*Sai Kiran Sharma[1,3], Kuntal K. Sevak[1], Sebastien Monette[2], Sean D. Carlin[1], James C. Knight[3], Frank R. Wuest[3], Evis Sala[4], Brian M. Zeglis[5], Jason S. Lewis[1]*

## SUPPLEMENTARY METHODS

### Cell Lines and Culture

Human ovarian adenocarcinoma OVCAR3 and SKOV3 cells were obtained from American Type Culture Collection (ATCC, Manassas, VA). The cells were grown as adherent monolayers in a 37°C incubator providing humidified atmosphere of 5% $CO_2$ in air. OVCAR3 cells were cultured using RPMI 1640 medium supplemented with heat inactivated fetal bovine serum (20% v/v, GIBCO, Life Technologies), 2 mM L-glutamine, 10 mM HEPES, 1 mM sodium pyruvate, 4.5 g/L glucose, 1.5 g/L sodium bicarbonate, 0.01 mg/mL bovine insulin (Gemini Bio-Products, 700-112P), 100 units/mL penicillin and 100 µg/mL streptomycin. SKOV3 cells were cultured using McCoy's 5A medium supplemented with heat inactivated fetal bovine serum (10% v/v, GIBCO, Life Technologies), 1.5 mM L-glutamine, 2.2 g/L sodium bicarbonate, 100 units/mL penicillin and 100 µg/mL streptomycin. Adherent cells were harvested with 0.25% trypsin and 0.53 mM EDTA in Hank's Buffered Salt Solution (HBSS) without any traces of calcium or magnesium. The cells were passaged for sub-culturing at 70-80% confluence in a ratio of 1:2 to 1:4 (OVCAR3) and 1:3 to 1:6 (SKOV3).

**Animal Xenografts**

All animals were treated according to the guidelines approved by the Research Animal Resource Center and Institutional Animal Care and Use Committee at Memorial Sloan Kettering Cancer Center, NY. Female athymic nude mice (01B74-Athymic NCr-nu/nu, 20-22 gm, 6-8 week old) were obtained from National Cancer Institute and were allowed to acclimatize at the Memorial Sloan Kettering Cancer Center vivarium for 1 week before the implantation of xenografts. Mice were provided with food and water *ad libitum*. A total of $15 \times 10^6$ OVCAR3 cells suspended in 150 μL of 1:1 media/matrigel basement membrane matrix (BD Biosciences) were injected subcutaneously on the right shoulder. Due to the low *in vivo* tumorigenicity of OVCAR3 cells and a tendency of the tumor to regress temporarily after initial growth, a second inoculation of $10 \times 10^6$ OVCAR3 cells suspended in 150 μL of 1:1 media/ matrigel basement membrane matrix (BD Biosciences) was performed at the same site 10 days after the initial inoculation. Tumor growth was monitored daily, and tumor volume (V) was calculated using a vernier calipers and deduced using the formula: $V = \pi/6 \times \text{length} \times \text{width} \times \text{height}$. Mice were used for imaging and acute biodistribution studies after the tumor volumes reached 150-300 $mm^3$. Bilateral xenografts — OVCAR3 (CA125-positive) cells on the left shoulder and SKOV3 (CA125-negative) cells on the right shoulder — were implanted into an additional cohort of mice (n = 5) in order to provide an internal control for the *in vivo* evaluation of $^{89}$Zr-DFO-MAb-B43.13.

**Preparation of Radioimmunoconjugates**

CA125-targeting murine monoclonal antibody was produced from the B43.13 hybridoma (provided by Quest PharmaTech Inc., Canada) and purified by protein G affinity chromatography as described previously (*1*). To prepare high specific activity

radioimmunoconjugate, ten molar equivalents of *p*-isothiocyanatobenzoyl-desferrioxamine (*p*-SCN-DFO; Macrocyclics, Inc.) was mixed with one molar equivalent of MAb-B43.13 (Quest PharmaTech Inc., Canada) in 0.1 M sodium bicarbonate buffer pH 8.7. The reaction was allowed to proceed for 1 h at 37 °C before purifying the DFO-modified MAb-B43.13 (DFO-MAb-B43.13) via size exclusion chromatography using a PD-10 desalting column (Sephadex G-25 M, GE Healthcare) that was pre-equilibrated with phosphate buffered saline (PBS; pH 7.4). An isotype control IgG (Sigma-Aldrich, Inc.) was similarly modified with *p*-SCN-DFO and used for *in vitro* and *in vivo* studies. To radiolabel the immunoconjugates, the DFO-conjugated antibodies (300-400 μg) were first added to 200 μL buffer (PBS, pH 7.4). Then, in a separate vial, $^{89}$Zr-oxalate (74-95 MBq; 2-2.5 mCi) in 1.0 M oxalic acid was adjusted to pH 7.0-7.5 using 1.0 M sodium carbonate. The pH-adjusted $^{89}$Zr was then added to the antibody solution, and the mixture was incubated at room temperature for 1 h. The reaction progress was assayed via radio-thin layer chromatography (radio-TLC) on silica-impregnated paper using an eluent of 50 mM EDTA, pH 5. After 1 h, the reaction was quenched with 50 μL of the same EDTA solution, and the radioimmunoconjugate was purified using a PD-10 desalting column for size-exclusion chromatography. The radiochemical purity of the crude and final radioimmunoconjugates was assayed by radio-TLC. In the TLC experiments, the radiolabeled antibody construct remains at the baseline, while $^{89}Zr^{4+}$ ions and $^{89}$Zr-EDTA elute with the solvent front. All experiments were performed in triplicate.

**Functional Characterization of $^{89}$Zr-DFO-MAb-B43.13**

The $^{89}$Zr-DFO-MAb-B43.13 radioimmunoconjugate was functionally characterized for the selective binding to antigen-expressing cells and the determination of the immunoreactive

fraction via Lindmo assays and antigen saturation binding assays (*2*). The *in vitro* stability of $^{89}$Zr-DFO-MAb-B43.13 with respect to radiochemical purity and demetallation was verified by incubating the radioimmunoconjugate in human AB-type serum for 7 days at 37 °C and assaying the radiochemical purity daily via radio-TLC.

**Lindmo assay:** OVCAR3 cells were aliquoted into microcentrifuge tubes at concentrations of 5, 4, 3, 2.5, 2, 1.5 and 0.5 x $10^6$ cells in 500 µl PBS (pH 7.4). A stock solution of the $^{89}$Zr-DFO-MAb-B43.13 radioimmunoconjugate was prepared in PBS (pH 7.4) supplemented with 1% bovine serum albumin (BSA) such that 50 µl of this solution measured 20,000 cpm on a gamma counter. 50 µl aliquots of $^{89}$Zr-DFO-MAb-B43.13 were uniformly aliquoted into the aforementioned tubes containing OVCAR3 cells. This setup was allowed to incubate for 1 hr at room temperature on a platform mixer. Thereafter, OVCAR3 cells were pelleted by centrifugation (600 x g for 3 min), followed by two rinses with ice cold PBS before aspirating out the supernatant and measuring cell-bound radioactivity on a gamma counter (Wizard$^{2®}$ 2480 Automatic Gamma Counter, Perkin-Elmer). The resulting data was background corrected, and compared with counts from the total activity added control samples in the experiments. A similar set up was organized to conduct experiments using CA125-negative SKOV3 cells. The immunoreactive fraction was determined by performing a linear regression analysis on a double-inverse plot of (total/bound) activity versus normalized cell concentration. The immunoreactive fraction was obtained from the inverse of the intercept on the plot. All data was obtained in triplicates and no weighting was applied.

**Antigen Saturation Binding Assay**: The *in vitro* immunoreactivity of $^{89}$Zr-DFO-MAb-B43.13 for OVCAR3 cells was further confirmed using an antigen saturation-binding assay. To this end, a 0.4 μg/mL solution of $^{89}$Zr-DFO-MAb-B43.13 was prepared in PBS supplemented with 1% BSA. Twenty microliters of the radioimmunoconjugate solution was added to a microcentrifuge tube containing 10 x $10^6$ cells in 200 μL of culture media. The resulting mixture was incubated for 1 h on ice with intermittent tapping to resuspend the cells. Thereafter, the cells were pelleted via centrifugation (600 x g for 3 min), and the supernatant was pipetted out in to a separate microcentrifuge tube. The cells were washed with 1 mL of ice-cold PBS, and centrifuged (600 × g for 3 min) before pipetting out the supernatant to another centrifuge tube. This washing procedure was repeated two more times. Finally, the cell pellet, the media supernatant, and the three wash fractions were measured for radioactivity on a gamma counter calibrated for $^{89}$Zr. The immunoreactive fraction of the radioimmunoconjugate was determined using the formula:

$$\text{Immunoreactive Fraction} = [\text{Counts}_{\text{Cell Pellet}}]/[[\text{Counts}_{\text{Cell Pellet}} + \text{Counts}_{\text{Media Supernatant}} + \text{Counts}_{\text{Wash1}} + \text{Counts}_{\text{Wash2}} + \text{Counts}_{\text{Wash3}}]$$

No weighting was applied to the data, and the data were obtained in triplicate.

**PET Imaging**

A minimum of 20 million coincident events was recorded for each scan, which lasted between 10-45 min. An energy window of 350-700 keV and a coincidence-timing window of 6 ns were used. The counting rates in the reconstructed images were converted to activity concentrations (percentage injected dose [%ID] per gram of tissue) by use of a system calibration factor derived from the imaging of a mouse-sized water-equivalent phantom containing $^{89}$Zr. Data were sorted into 2-dimensional histograms by Fourier re-binning, and transverse images were reconstructed

by filtered back-projection (FBP) into a 128 × 128 × 63 (0.72 × 0.72 × 1.3 mm) matrix. The image data were normalized to correct for non-uniformity of response of the PET, dead-time count losses, positron branching ratio, and physical decay to the time of injection, but no attenuation, scatter, or partial-volume averaging correction was applied.

**Acute Biodistribution**

Acute *in vivo* biodistribution studies were performed to evaluate the uptake of $^{89}$Zr-DFO-MAb-B43.13 and $^{89}$Zr-DFO-IgG in mice bearing subcutaneous OVCAR3 xenografts (right shoulder; 150-300 mm$^3$; 8-10 weeks post inoculation). Tumor-bearing mice were warmed gently under a heat lamp for 5 min before administration of the appropriate $^{89}$Zr-DFO-immunoconjugate [0.55 – 0.75 MBq (15-20 μCi) in 200 μL 0.9% sterile saline, 4-6 μg] via intravenous tail vein injection (t = 0). Animals (n = 4 per group) were euthanized by $CO_2$(g) asphyxiation at 24, 48, 72, 96, and 120 h post-injection. To probe the ability to saturate the biomarker, an additional cohort of animals were administered $^{89}$Zr-DFO-MAb-B43.13 with dramatically lowered specific activity — achieved by co-injection of the standard dose of $^{89}$Zr-DFO-MAb-B43.13 mixed with 480 μg of the cold, unlabeled DFO-MAb-B43.13 — and euthanized at 72 h post-injection. After asphyxiation, relevant tissues (including tumor) were removed, rinsed in water, dried in air for 5 min, weighed, and counted in a gamma counter calibrated for $^{89}$Zr. Counts were converted into activity using a calibration curve generated from known standards. Count data were background- and decay-corrected to the time of injection, and the %ID/g for each tissue sample was calculated by normalization to the total activity injected.

**Ex Vivo Analyses**

Upon euthanizing the OVCAR3 tumor-bearing mice (n=7), necropsy was performed to harvest the xenografts and selected lymph nodes. One set of tissues was frozen in OCT medium for autoradiography, while the other was fixed in 10% neutral buffered formalin for histopathological analyses. Cryosectioning and digital autoradiography of the frozen tissues was carried out as previously described, with the exception of the plate reader in this instance being a GE Typhoon 7000IP with maximum pixel resolution of 25 μm.(*3*) Sequential tumor sections were analyzed by staining with hematoxylin and eosin (H&E), and the images were captured as described previously (*3*). Immunofluorescence was performed on frozen sections by staining for CA125 using a 1:250 dilution of the primary antibody (Novus Biologicals, NBP1-96619) in 2% BSA/PBS, and secondary Alexa-Fluor 488-conjugated antibody (Life Technologies Cat. A21206) diluted in 1% BSA/PBS. The slides were digitized by Pannoramic Flash scanners (3DHistech), using 20x/0.8NA objective and with DAPI and FITC filter cubes. Scanned images were viewed and exported using Pannoramic Viewer software (3DHistech), adjusted for visual quality, and registered using ImageJ software.

For histopathology, the formalin fixed tissues were processed in ethanol and xylene, embedded in paraffin, sectioned at 5 μm thickness, and stained with hematoxylin and eosin. The harvested lymph nodes were sectioned at 5 different levels and analyzed for histopathology at each level in order to achieve thorough coverage of the nodes. Sections from the tumor and selected lymph nodes were stained by immunohistochemistry (IHC) for CA125/MUC16 on a Leica Bond RX automated staining platform (Leica Biosystems). Following heat-induced epitope retrieval in a pH 9.0 buffer, the primary antibody (Novus Biologicals, NBP1-96619) was applied at a concentration of 1:250 and was followed by application of a polymer detection

system (Novocastra Bond Polymer Refine Detection, Leica Biosystems, DS9800). All slides were evaluated by a board-certified veterinary pathologist (S.M.).

**CA125 ELISA**: Serum samples from OVCAR3 tumor bearing mice and spent media from OVCAR3 and SKOV3 cell cultures were assayed in a sandwich ELISA to quantify the amount of shed antigen (Abnova, Inc.). Considering the physical half-life of $^{89}$Zr and the *in vivo* biological clearance of antibodies, tumor-bearing mice injected with $^{89}$Zr-DFO-MAb-B43.13 for PET imaging were euthanized 4-5 weeks after the administration of the radioimmunoconjugate. This ensured that the serum samples used for ELISA were not radioactive and minimized the likelihood of the presence of any circulating CA125::$^{89}$Zr-DFO-MAb-B43.13 immunocomplexes, which could invalidate the quantification of CA125 in the serum samples.

## SUPPLEMENTAL RESULTS

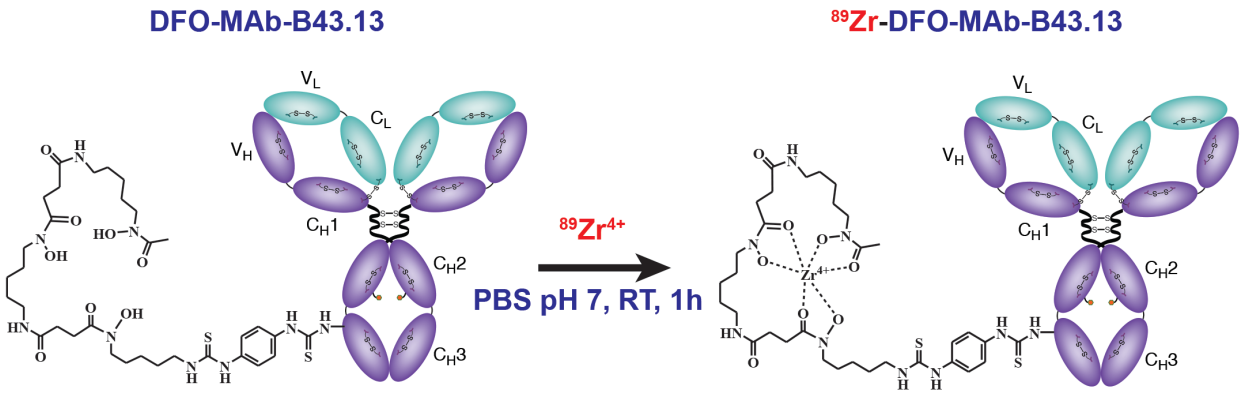


**Supplemental Fig. 1. $^{89}$Zr-Radiolabeling of DFO-MAb-B43.13:** Schematic of the radiolabeling of DFO-MAb-B43.13 immunoconjugate with $^{89}$Zr.

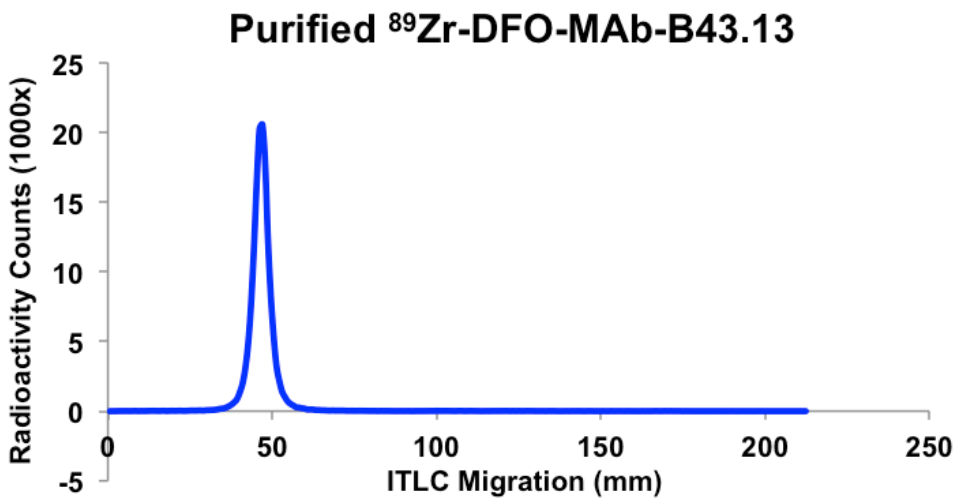


**Supplemental Fig. 2. Radiochemical Purity of the Radioimmunoconjugate:** The size-exclusion purified $^{89}$Zr-DFO-MAb-B43.13 was tested for radiochemical purity via radio-TLC. The ratio of radioactivity at the baseline (~50 mm) versus the eluent front (~200 mm) indicates the purity of the preparation.

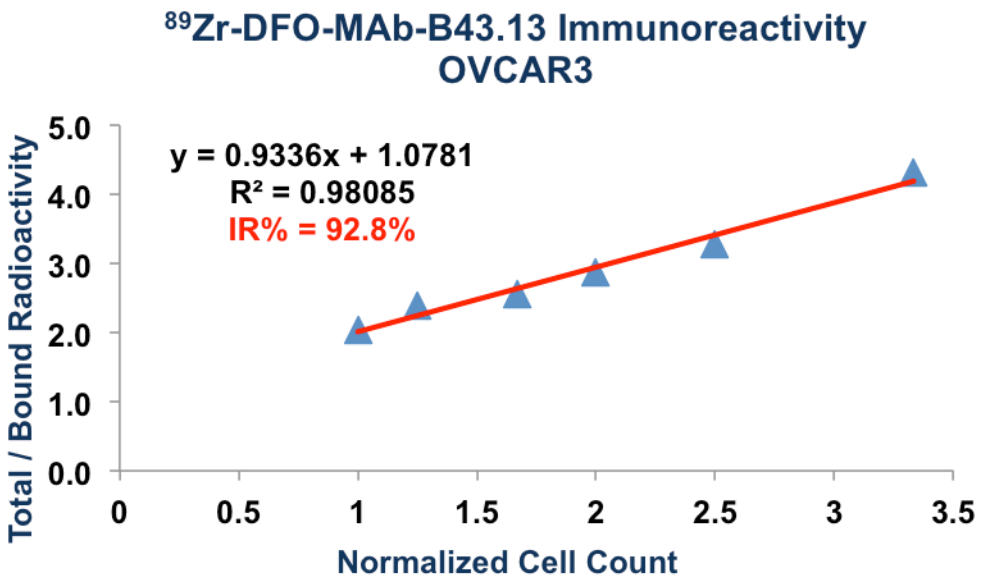


**Supplemental Fig. 3. Determination of the Immunoreactivity of $^{89}$Zr-DFO-MAB-B43.13 via Lindmo assay:** A representative double inverse plot to determine the immunoreactivity (%IR) of $^{89}$Zr-DFO-MAb-B43.13 using OVCAR3 cells.

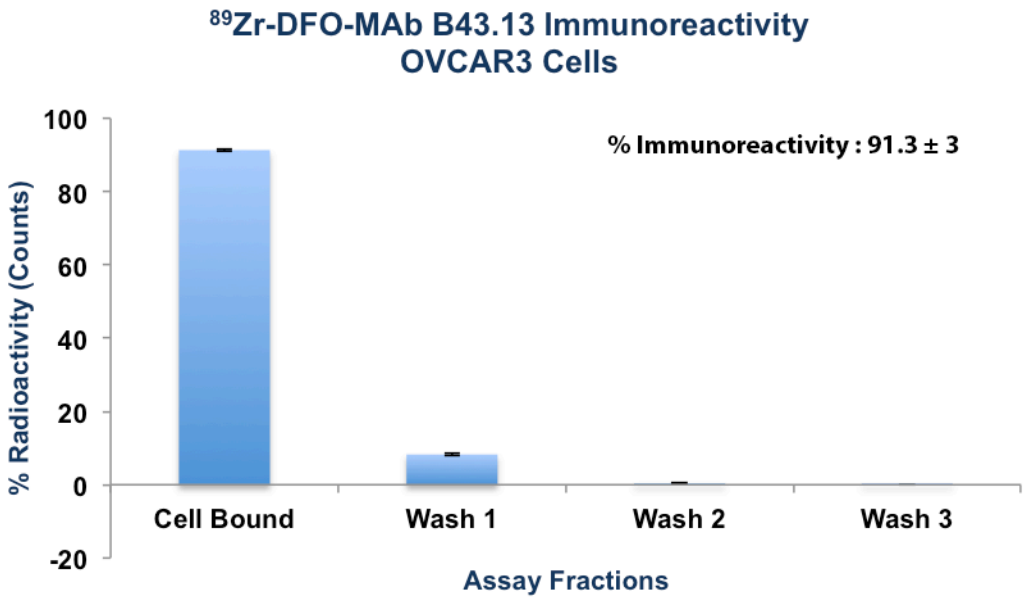


**Supplemental Fig. 4. Determination of the Immunoreactivity of $^{89}$Zr-DFO-MAB-B43.13 via Saturation Binding Assay:** The percentage cell-bound radioactivity is a direct measure of the immunoreactive fraction of $^{89}$Zr-DFO-MAb-B43.13

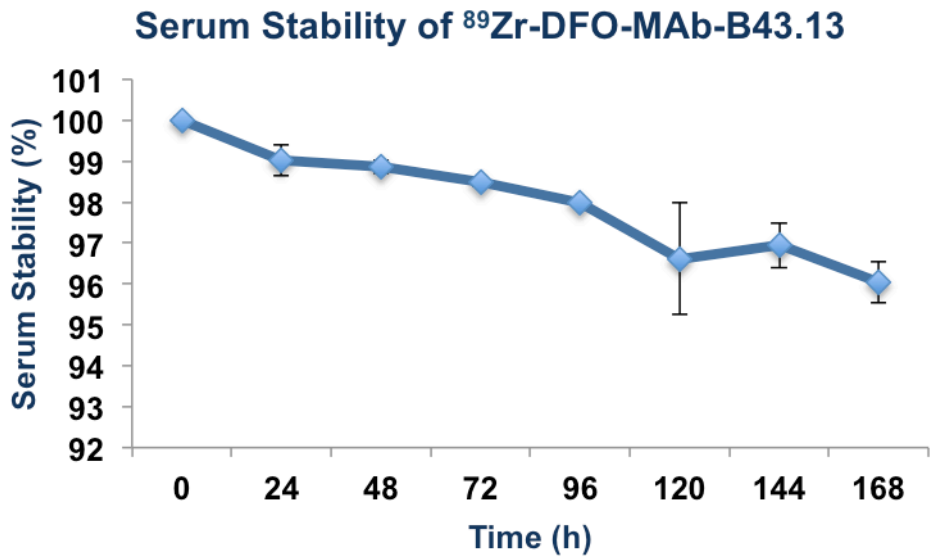


**Supplemental Fig. 5.** ***In vitro*** **Stability of the $^{89}$Zr-DFO-MAb-B43.13:** Line plot representing the serum stability of the radioimmunoconjugate over a period of 7 days.

**Supplemental Table 1:** *Ex vivo* biodistribution data for $^{89}$Zr-DFO-MAb-B43.13 versus time in mice bearing subcutaneous OVCAR3 xenografts (n = 4 for each time point). Mice were administered $^{89}$Zr-DFO-MAb-B43.13 [0.55 – 0.75 MBq (15-20 μCi) in 200 μL 0.9% sterile saline] via tail vein injection (t = 0). For the 72 h time point, an additional cohort of animals were given $^{89}$Zr-DFO-MAb-B43.13 with dramatically lowered specific activity (LSA), achieved by the co-injection of the standard dose of the $^{89}$Zr-labeled construct mixed with 480 μg of cold, unlabeled DFO-MAb-B43.13.

| | 24 h | 48 h | 72 h | 72 h block | 96 h | 120 h |
|---|---|---|---|---|---|---|
| ***Blood*** | 9.1 ± 0.6 | 6.2 ± 3.3 | 3.3 ± 1.6 | 7.2 ± 2.1 | 5.2 ± 2.8 | 4 ± 3 |
| ***Tumor*** | 7.2 ± 0.3 | 19.3 ± 4.8 | 22.3 ± 6.3 | 7.6 ± 3.2 | 19.2 ± 3.1 | 24.7 ± 7.5 |
| ***Heart*** | 3.2 ± 0.6 | 2.6 ± 1.1 | 1.6 ± 0.5 | 3.2 ± 0.5 | 2.2 ± 1.1 | 1.7 ± 1 |
| ***Lung*** | 2.4 ± 0.6 | 3.1 ± 2.1 | 1.4 ± 0.8 | 3.2 ± 2 | 2.2 ± 0.5 | 2 ± 1.9 |
| ***Liver*** | 14.9 ± 8 | 13.3 ± 8.8 | 12.7 ± 6.4 | 15.4 ± 5.6 | 14.7 ± 2.1 | 16.8 ± 5.7 |
| ***Spleen*** | 2.6 ± 1.6 | 2.5 ± 1 | 2.6 ± 1.7 | 4.2 ± 1.8 | 2.9 ± 2 | 4.8 ± 2 |
| ***Stomach*** | 1.0 ± 0.6 | 0.2 ± 0.1 | 0.5 ± 0.4 | 0.9 ± 0.3 | 0.5 ± 0.2 | 0.2 ± 0.1 |
| ***Large Intestine*** | 1.1 ± 0.3 | 0.6 ± 0.2 | 0.5 ± 0.2 | 0.8 ± 0.1 | 0.6 ± 0.2 | 0.4 ± 0.3 |
| ***Small Intestine*** | 0.9 ± 0.3 | 0.7 ± 0.1 | 0.5 ± 0.1 | 1 ± 0.1 | 0.7 ± 0.2 | 0.6 ± 0.6 |
| ***Kidney*** | 4.2 ± 0.7 | 4 ± 0.8 | 3.5 ± 0.9 | 4 ± 1.2 | 3.9 ± 1.7 | 3 ± 1.3 |
| ***Uterus/Ovaries*** | 2.2 ± 2.1 | 1.0 ± 0.3 | 1.0 ± 0.3 | 2.4 ± 1.4 | 2.9 ± 2.2 | 2.4 ± 2.3 |
| ***Muscle*** | 0.4 ± 0.2 | 0.3 ± 0.1 | 0.2 ± 0.1 | 0.2 ± 0.1 | 0.1 ± 0.1 | 0.1 ± 0.1 |
| ***Bone*** | 0.6 ± 0.2 | 1.1 ± 0.2 | 0.9 ± 0.4 | 0.7 ± 0.6 | 0.6 ± 0.6 | 0.5 ± 0.4 |

**Supplemental Table 2:** Tumor-to-Tissue radioactivity ratios for $^{89}$Zr-DFO-MAb-B43.13 versus time in mice bearing subcutaneous OVCAR3 xenografts (n = 4 for each time point).

| | 24 h | 48 h | 72 h | 72 h block | 96 h | 120 h |
|---|---|---|---|---|---|---|
| **Tumor/Blood** | 0.8 ± 0.1 | 3.1 ± 1.8 | 6.8 ± 3.8 | 1.0 ± 0.5 | 3.7 ± 2.1 | 6.2 ± 5.0 |
| **Tumor/Heart** | 2.2 ± 0.4 | 7.3 ± 3.6 | 13.5 ± 5.4 | 2.4 ± 1.1 | 8.7 ± 4.6 | 14.7 ± 10.0 |
| **Tumor/Lung** | 3 ± 0.8 | 6.3 ± 4.5 | 15.6 ± 10 | 2.4 ± 1.8 | 8.6 ± 2.5 | 12.2 ± 12.0 |
| **Tumor/Liver** | 0.5 ± 0.3 | 1.5 ± 1.0 | 1.8 ± 1.0 | 0.5 ± 0.3 | 1.3 ± 0.3 | 1.5 ± 0.7 |
| **Tumor/Spleen** | 2.8 ± 1.7 | 7.8 ± 3.7 | 8.7 ± 6.3 | 1.8 ± 1.1 | 6.7 ± 4.8 | 5.2 ± 2.7 |
| **Tumor/Stomach** | 7.4 ± 4.5 | 83.9 ± 55.7 | 41.8 ± 32.3 | 8.6 ± 4.9 | 38.5 ± 18.5 | 106.1 ± 65.4 |
| **Tumor/Large Intestine** | 6.8 ± 2 | 32.4 ± 11.5 | 45.9 ± 20.6 | 9.8 ± 4.3 | 30.9 ± 10.1 | 61.4 ± 49.7 |
| **Tumor/Small Intestine** | 7.9 ± 2.6 | 29.6 ± 9.6 | 43.4 ± 16.7 | 7.3 ± 3.3 | 25.6 ± 7.4 | 38.9 ± 38.1 |
| **Tumor/Kidney** | 1.7 ± 0.3 | 4.8 ± 1.6 | 6.5 ± 2.4 | 1.9 ± 1.0 | 4.9 ± 2.3 | 8.1 ± 4.3 |
| **Tumor/Uterus + Ovary** | 3.2 ± 3.1 | 19.3 ± 7.0 | 21.5 ± 8 | 3.1 ± 2.3 | 6.6 ± 5.3 | 10.5 ± 10.8 |
| **Tumor/Muscle** | 18.5 ± 8.5 | 60.4 ± 23.6 | 114.4 ± 46.6 | 47.5 ± 24.7 | 171.2 ± 144.9 | 565.4 ± 256.2 |
| **Tumor/Bone** | 12.6 ± 4.6 | 18.2 ± 6.1 | 25.7 ± 13.1 | 10.3 ± 9.3 | 32 ± 33.8 | 48.4 ± 44.3 |

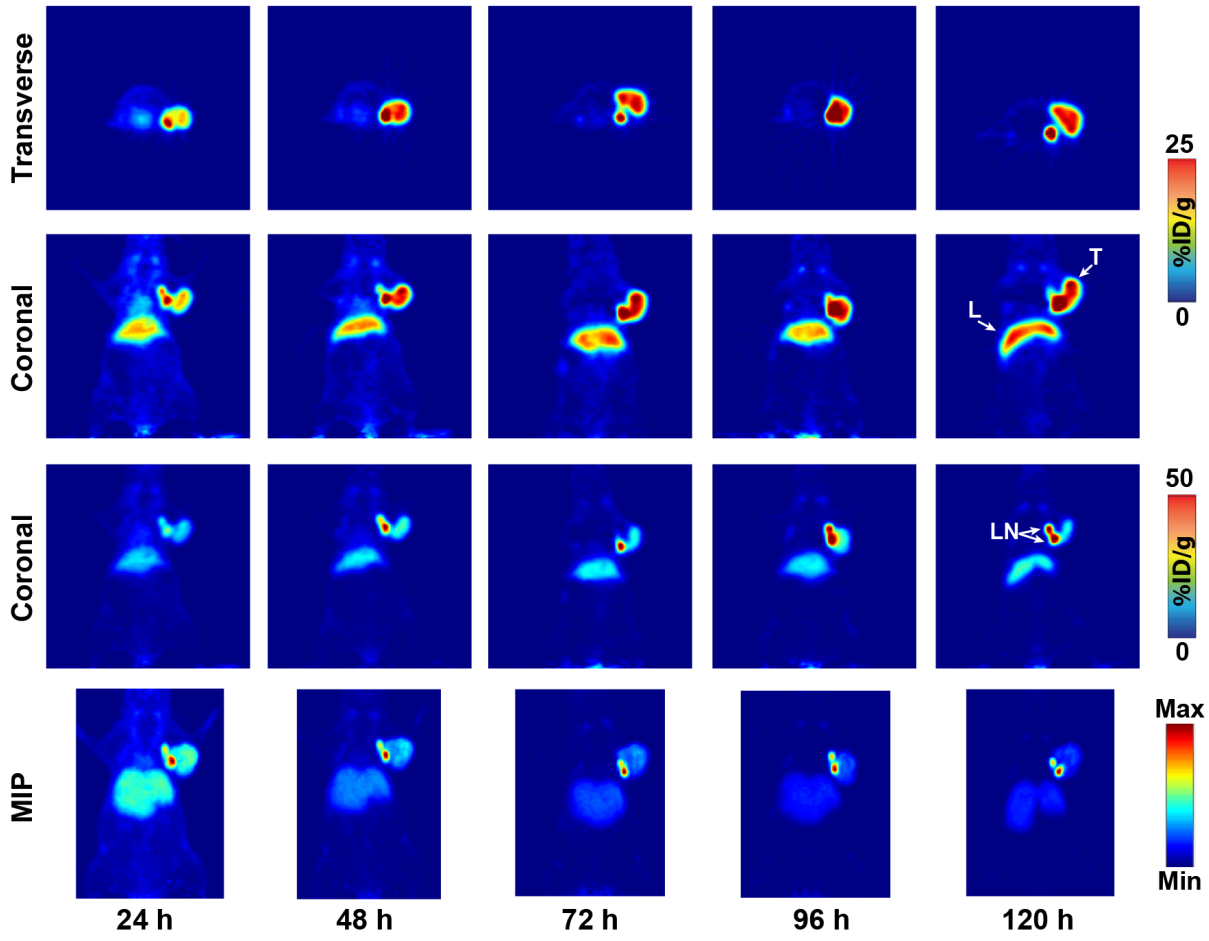


**Supplemental Fig. 6. Small Animal PET Imaging of OVCAR3 Tumors with $^{89}$Zr-DFO-MAb-B43.13:** Serial PET images of $^{89}$Zr-DFO-MAb-B43.13 [10.2 – 12.0 MBq (275-325 µCi) injected via tail vein in 200 µL 0.9 % sterile saline] in an athymic nude mouse (shown in Fig. 4A) bearing subcutaneous CA125-positive OVCAR3 xenograft on the right shoulder. PET imaging was performed at 24 h intervals up to 120 h post-injection of $^{89}$Zr-DFO-MAb-B43.13. The lowermost panel represents maximum intensity projection (MIP) images for all corresponding time points of evaluation. Arrows indicate the tumor (T), liver (L), and lymph nodes (LN).

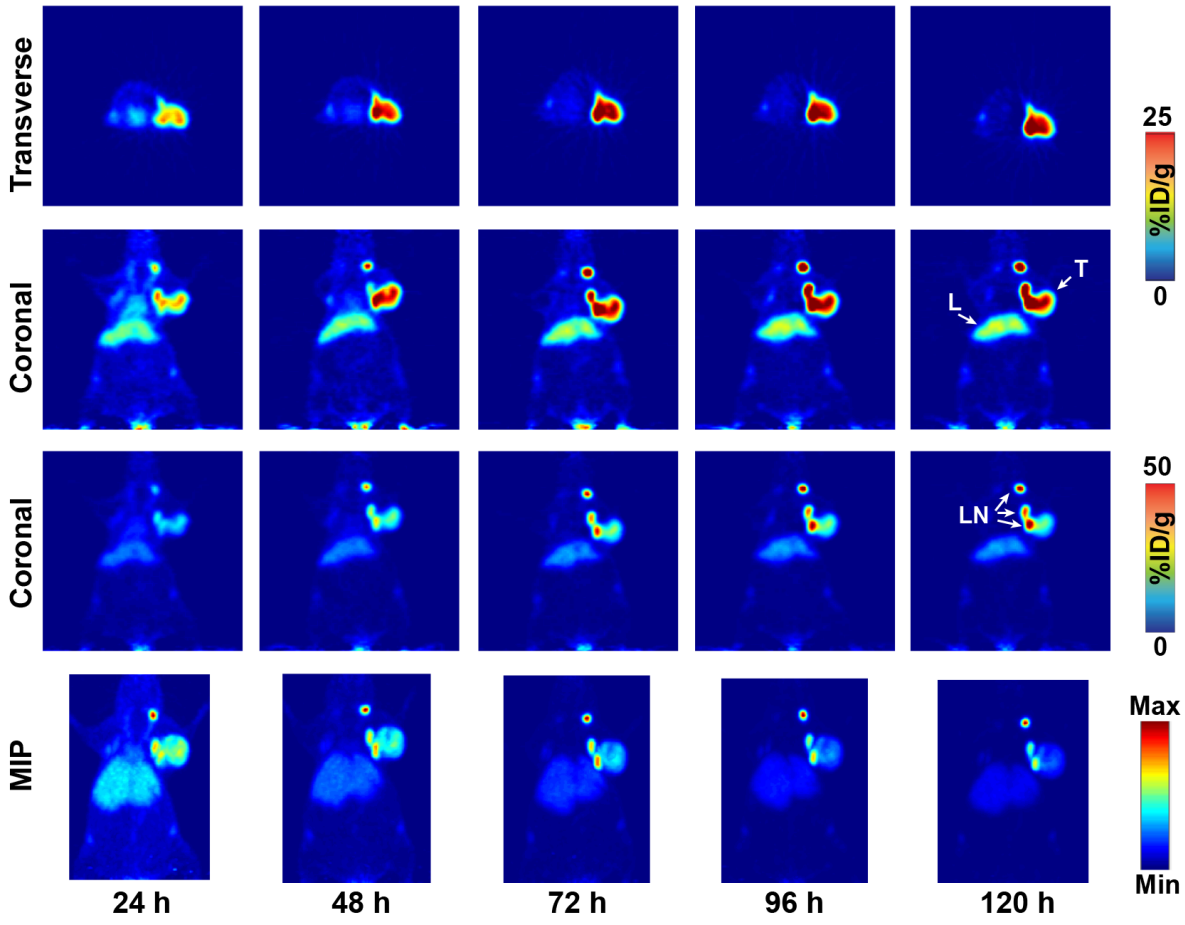


**Supplemental Fig. 7. Small Animal PET Imaging of OVCAR3 Tumors with $^{89}$Zr-DFO-MAb-B43.13:** PET images of $^{89}$Zr-DFO-MAb-B43.13 [10.2 – 12.0 MBq (275-325 µCi) injected via tail vein in 200 µL 0.9 % sterile saline] in another athymic nude mouse (shown in Fig. 4A) bearing subcutaneous CA125-positive OVCAR3 xenograft on the right shoulder. PET imaging was performed at 24 h intervals up to 120 h post-injection of $^{89}$Zr-DFO-MAb-B43.13. The lowermost panel represents maximum intensity projection (MIP) images for all corresponding time points of evaluation. Arrows indicate the tumor (T), liver (L), and lymph nodes (LN).

**Supplemental Table 3:** *Ex vivo* biodistribution data for $^{89}$Zr-DFO-MAb-B43.13, and $^{89}$Zr-DFO-IgG at 120 h post-injection in mice bearing subcutaneous OVCAR3 xenografts (n=4). Mice were administered $^{89}$Zr-DFO-MAb-B43.13 or $^{89}$Zr-DFO-IgG (0.55 – 0.75 MBq [15-20 μCi] in 200 μL 0.9% sterile saline) via tail vein injection (t = 0).

| | $^{89}$Zr-DFO-MAb-B43.13 | $^{89}$Zr-DFO-IgG |
|---|---|---|
| ***Blood*** | 1.3 ± 1 | 9.9 ± 0.6 |
| ***Tumor*** | 18 ± 3.4 | 6.1 ± 0.4 |
| ***Proximal Brachial Node*** | 56.6 ± 39.4 | 6.1 ± 5 |
| ***Proximal Axillary Node*** | 104.8 ± 45.1 | 2.1 ± 0.9 |
| ***Distal Brachial Node*** | 6.4 ± 3.7 | 6 ± 2.7 |
| ***Distal Axillary Node*** | 3.7 ± 3.2 | 5.6 ± 4.5 |

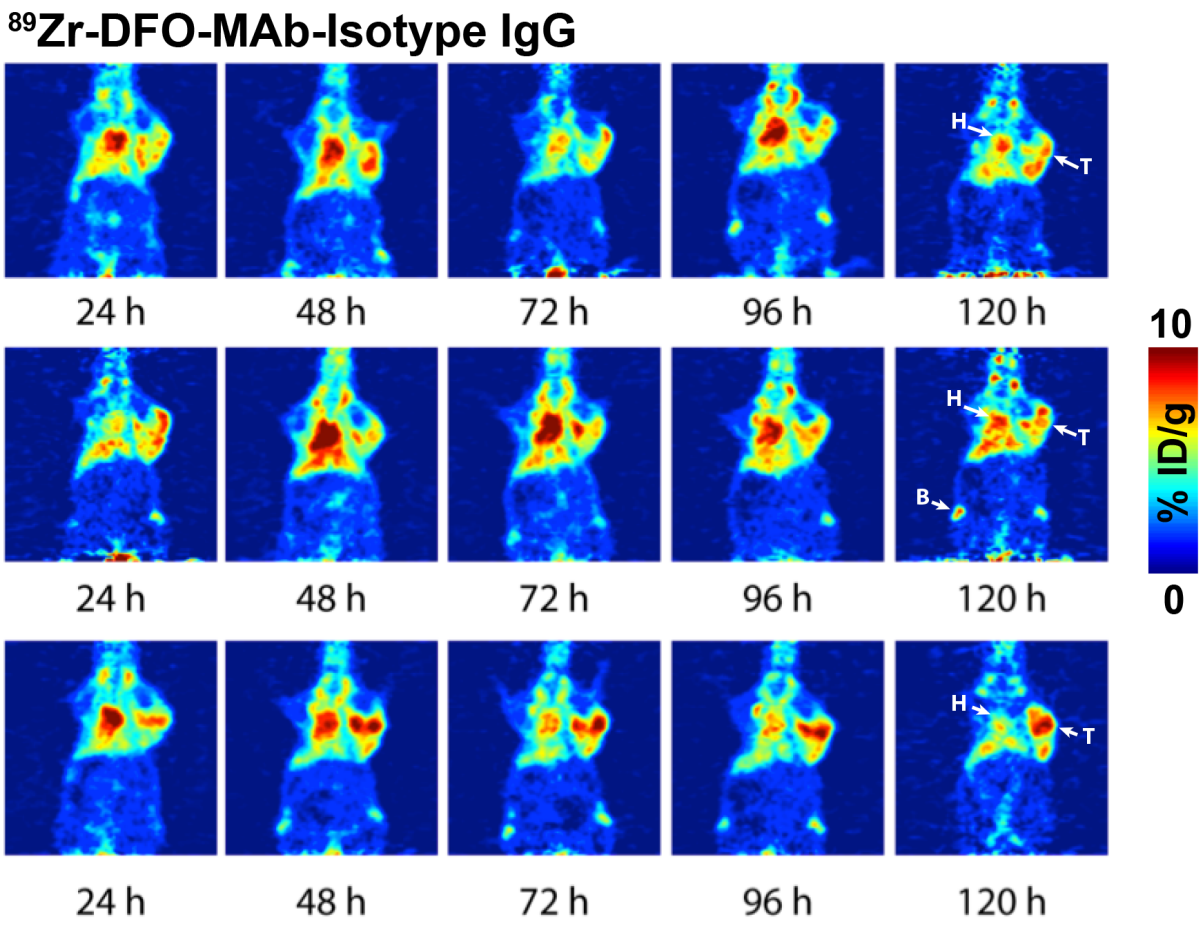


**Supplemental Fig. 8. Small Animal PET imaging Analysis to Investigate Lymph Node Involvement:** Coronal PET images of $^{89}$Zr-DFO-IgG [7 – 9 MBq (190-243 µCi) injected via tail vein in 200 µL 0.9 % sterile saline] in athymic nude mice (n = 3) bearing subcutaneous CA125-expressing OVCAR3 tumors. PET imaging was performed at 24 h intervals up to 120 h post-injection of $^{89}$Zr-DFO-IgG. Images are scaled to 10 % ID/g to delineate the EPR-based non-specific uptake of the isotype IgG within OVCAR3 tumors, and to demonstrate its relatively higher persistence, distribution, and clearance profile from the systemic circulation of the animal. Arrows in the figures indicate the following: tumor (T), heart (H), and bone (B).

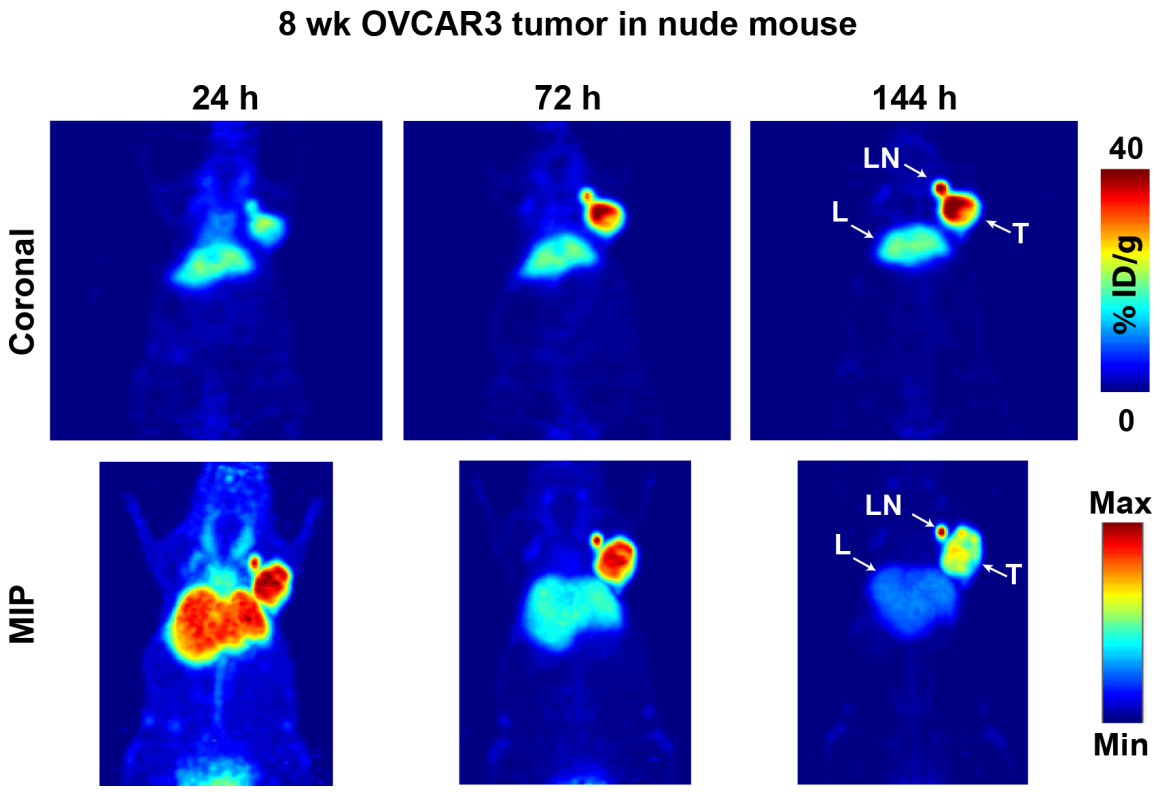


**Supplemental Fig. 9. Small Animal PET imaging of OVCAR3 Tumor with $^{89}$Zr-DFO-MAb-B43.13:** Coronal and Maximum Intensity Projection (MIP) serial PET images of $^{89}$Zr-DFO-MAb-B43.13 [10.2 – 12.0 MBq (275-325 μCi) injected via tail vein in 200 μL 0.9 % sterile saline] in athymic nude mouse bearing an 8-week old subcutaneous CA125-positive OVCAR3 xenograft on the right shoulder. PET imaging was performed at 24, 72 and 144 h post-injection of $^{89}$Zr-DFO-MAb-B43.13. Arrows indicate the following: tumor (T), liver (L), and lymph node (LN).

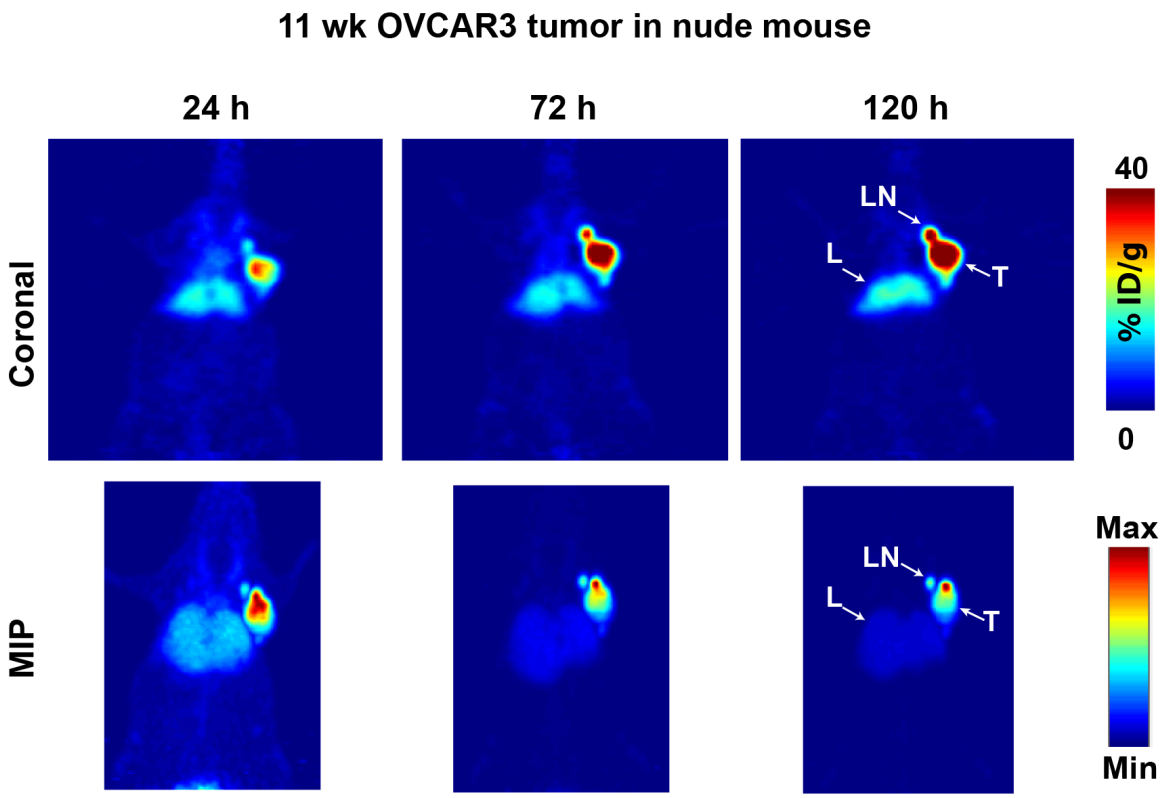


**Supplemental Fig. 10. Small Animal PET imaging of OVCAR3 Tumor with $^{89}$Zr-DFO-MAb-B43.13:** Coronal and Maximum Intensity Projection (MIP) serial PET images of $^{89}$Zr-DFO-MAb-B43.13 [10.2 – 12.0 MBq (275-325 µCi) injected via tail vein in 200 µL 0.9 % sterile saline] in the same athymic nude mouse as shown in Fig. S9, now bearing a 11-week old subcutaneous CA125-positive OVCAR3 tumor on the right shoulder. No progression of metastasis was observed in the ipsilateral sub-mandibular lymph node of this mouse even after 11 weeks. PET imaging was performed at 24, 72 and 120 h post-injection of $^{89}$Zr-DFO-MAb-B43.13. Arrows indicate the following: tumor (T), liver (L), and lymph node (LN).

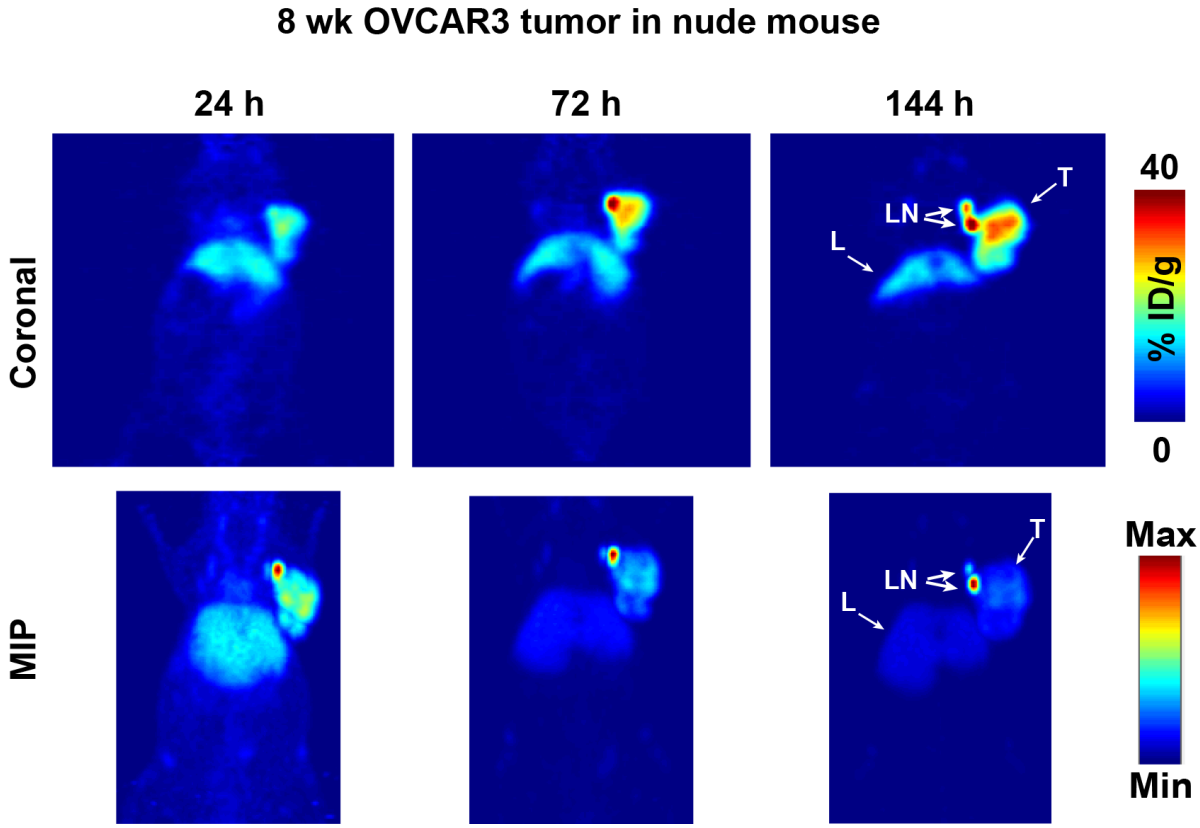


**Supplemental Fig. 11. Small Animal PET imaging of OVCAR3 Tumor with $^{89}$Zr-DFO-MAb-B43.13:** Coronal and Maximum Intensity Projection (MIP) serial PET images of $^{89}$Zr-DFO-MAb-B43.13 [10.2 – 12.0 MBq (275-325 µCi) injected via tail vein in 200 µL 0.9 % sterile saline] in athymic nude mouse bearing an 8-week old subcutaneous CA125-positive OVCAR3 xenograft on the right shoulder. PET imaging was performed at 24, 72 and 144 h post-injection of $^{89}$Zr-DFO-MAb-B43.13. Arrows indicate the following: tumor (T), liver (L), and lymph nodes (LN).

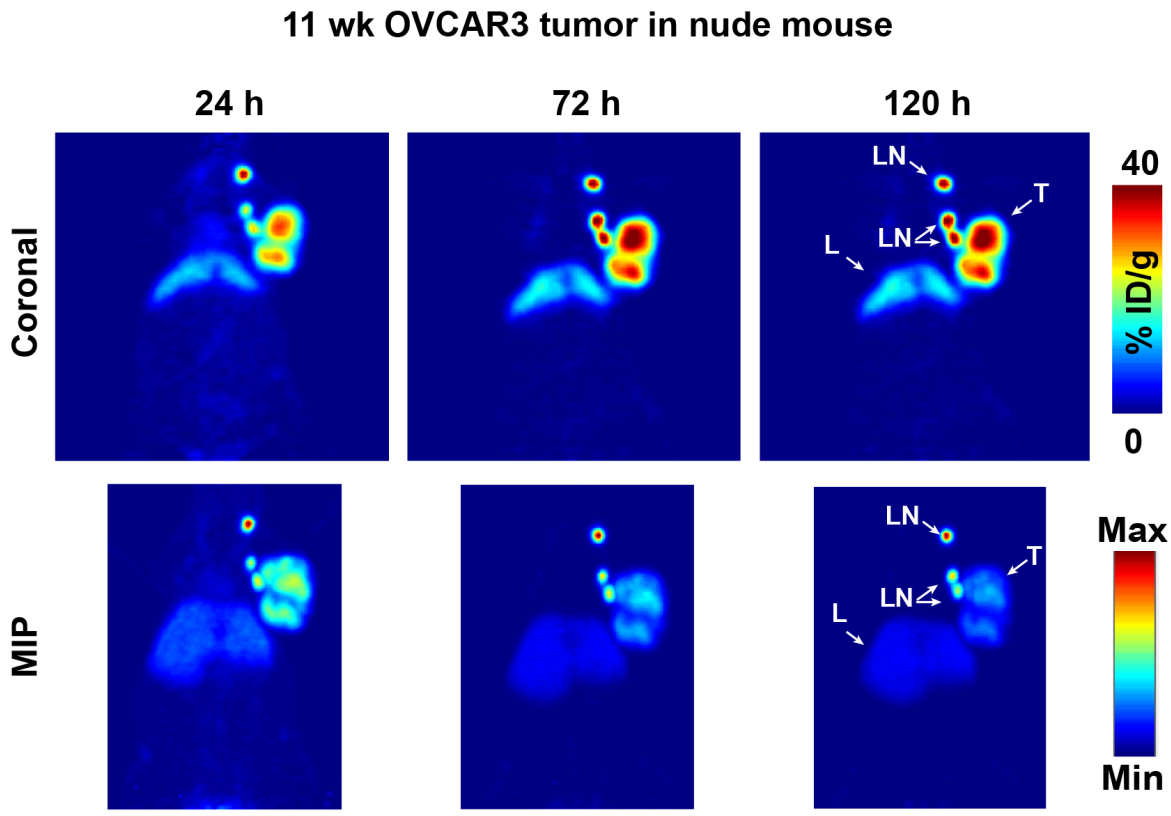


**Supplemental Fig. 12. Small Animal PET imaging of OVCAR3 Tumor with $^{89}$Zr-DFO-MAb-B43.13:** Coronal and Maximum Intensity Projection (MIP) serial PET images of $^{89}$Zr-DFO-MAb-B43.13 [10.2 – 12.0 MBq (275-325 µCi) injected via tail vein in 200 µL 0.9 % sterile saline] in the same athymic nude mouse as shown in Fig. S11, now bearing a 11-week old subcutaneous CA125-positive OVCAR3 xenografts on the right shoulder. This animal showed progression of lymph node metastasis to the ipsilateral sub-mandibular lymph node. PET imaging was performed at 24, 72 and 120 h post-injection of $^{89}$Zr-DFO-MAb-B43.13. Arrows indicate the following: tumor (T), liver (L), and lymph nodes (LN).

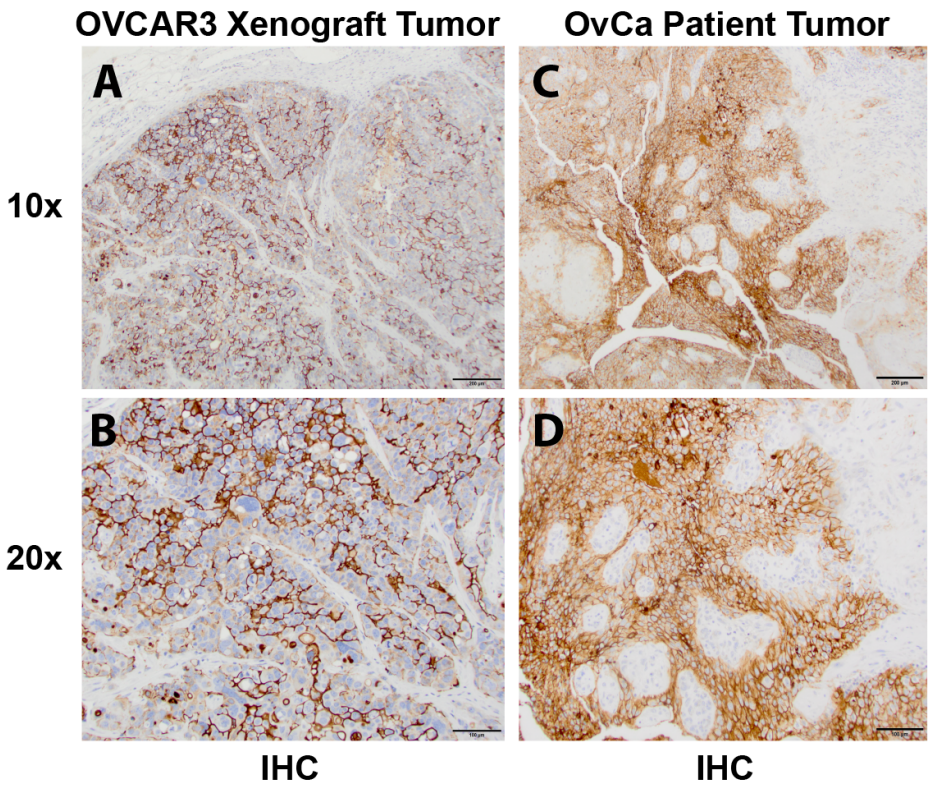


**Supplemental Fig. 13. Histopathologic Analysis of Ovarian Tumor Sections:** (A, B) 10x-, 20x-magnified images of immunohistochemical (IHC) staining of CA125 expression in OVCAR3 tumors harvested from the xenograft animal; (C, D) 10x-, 20x-magnified images of immunohistochemical (IHC) staining of CA125 expression in tumor sections biopsied from human patients with high grade serous ovarian cancer. The overall pattern of CA125 expression and staining was rich and similar between the two tumor tissues. CA125 expression was mostly membrane bound and distinctly outlines the ovarian cancer cells in the two tumor samples. The same primary antibody was used to stain both tumor sections. The scale bars for the 10x- and 20x-magnification images delineate 200 μm and 100 μm, respectively.

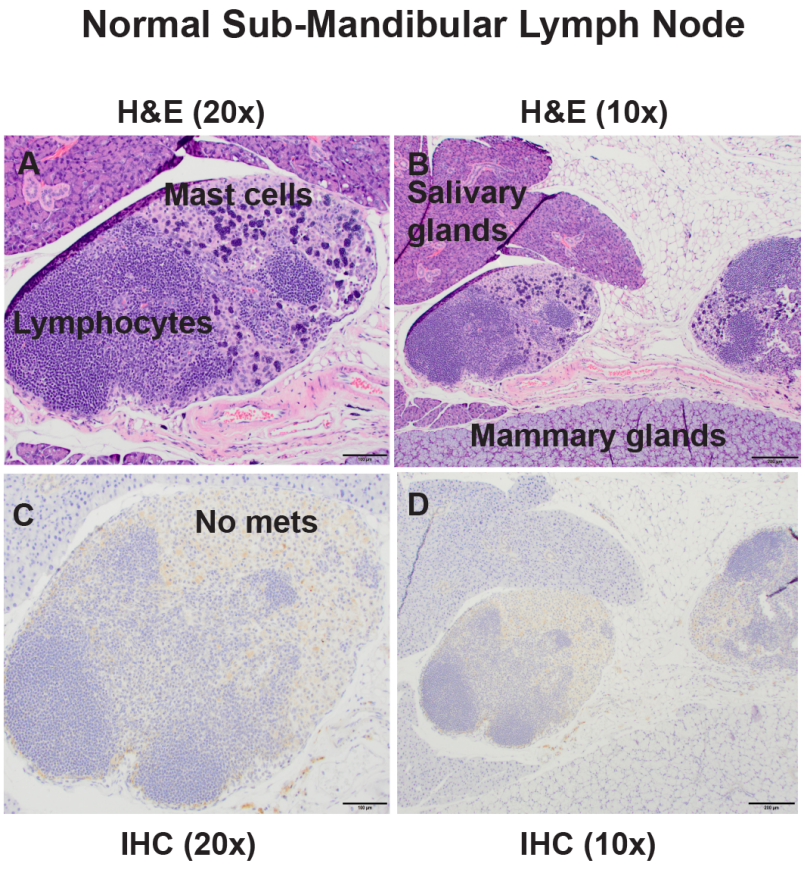


**Supplemental Fig. 14. Histopathological Analysis of the PET-Negative Sub-Mandibular Lymph Node Tissue:** (A) 20x- and (B) 10x-magnified images of H&E-stained sections of the immunoPET-negative sub-mandibular lymph node; (C) 20x- and (D) 10x-magnified images of the same lymph node, analyzed by immunohistochemical (IHC) staining for CA125 expression. In these images, the lymphocytes (stained blue) are seen in typical clusters along the sides of the node, mast cells are seen (dark-purple stained) as clusters in the H&E panels.

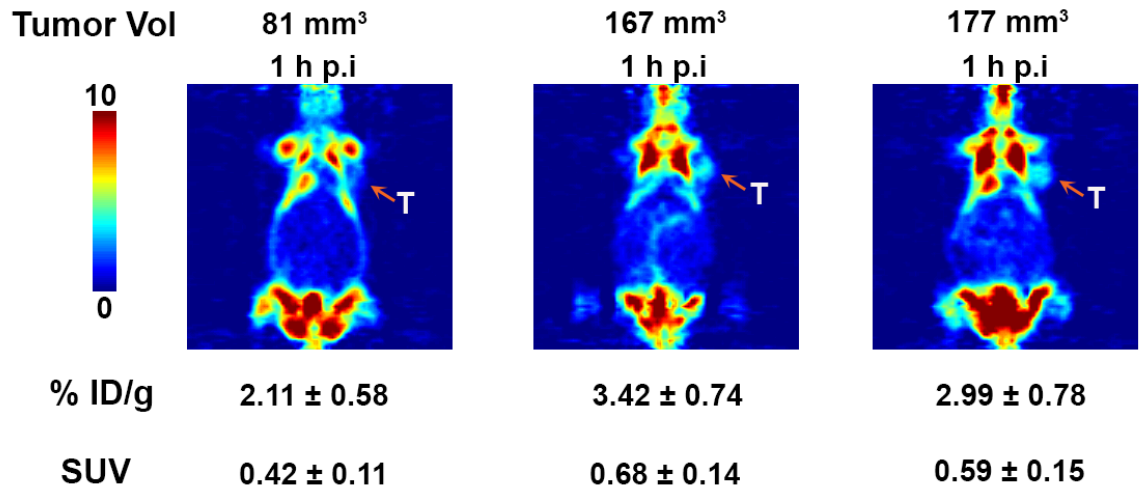


**Supplemental Fig. 15. $^{18}$F-FDG-PET" Imaging of OVCAR3 tumors:** Coronal images of OVCAR3 tumor bearing mice (n = 3). The animals were starved for 6 h prior to injection with ~ 9.25 MBq; (250 μCi) of "$^{18}$F-FDG" via the tail vein. Images were acquired 1 h after administration of the metabolic radiotracer. Orange arrows delineate the tumors. Uptake values for the radiotracer were obtained by drawing regions of interest (ROI) around delineated tumors in different coronal planes and applying statistics to the data. The uptake of "$^{18}$F-FDG" in OVCAR3 tumors matched well with values reported previously.

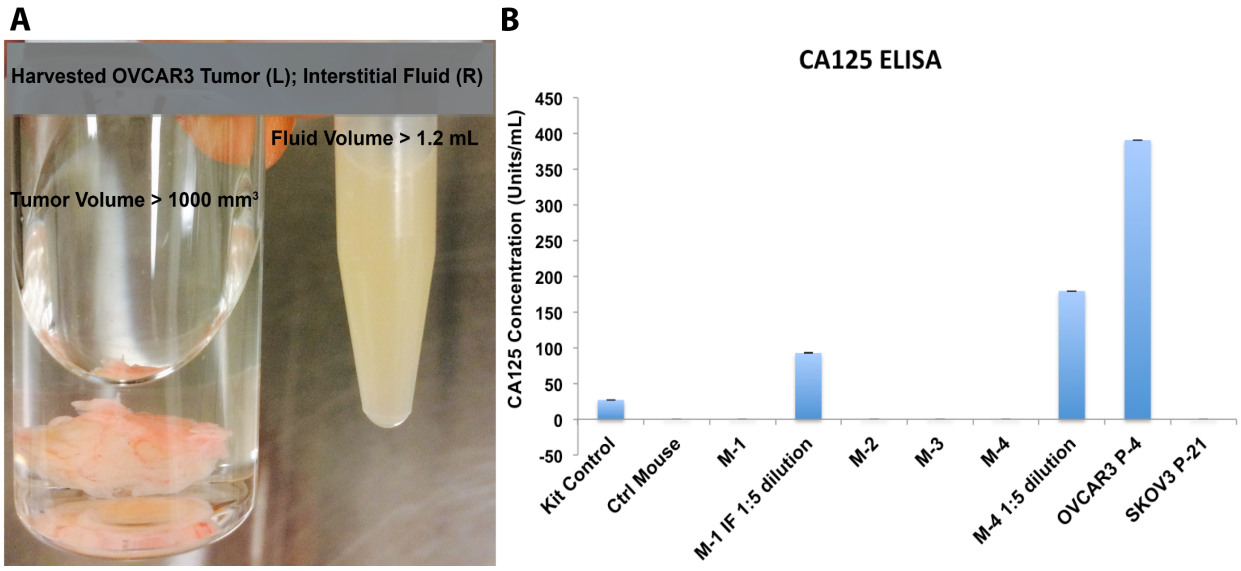


**Supplemental Fig. 16. *Ex vivo* Analyses of Serum and Tumor Interstitial Fluid:** (A) Left – a 5 mL glass vial containing an OVCAR3 tumor harvested from xenograft mouse (shown in Fig. S16); Right – Interstitial Fluid (IF) from within the tumor and surrounding it – collected in to a 1.5 mL microcentrifuge tube; (B) Graph of the results from CA125 ELISA assaying the following samples: kit supplied control, serum from healthy non-tumor bearing athymic nude mouse (Ctrl mouse), serum from OVCAR3 xenograft mice: M-1, M-2, M-3, M-4; 1:5 dilutions of tumor interstitial fluid (IF 1:5) from mice – M-1, and M-4; and spent culture media from OVCAR3 cells at passage 4 (P-4), and SKOV3 cells at passage 21 (P-21). None of the xenograft mice had any detectable levels of shed CA125 antigen in circulation. However, tumors from M-1 and M-4 had high volumes of interstitial fluid – rich in CA125 concentrations. Maximum CA125 concentration was observed in spent cell culture media of OVCAR3 cells, whereas no CA125 was detected in SKOV3 cell culture spent media.

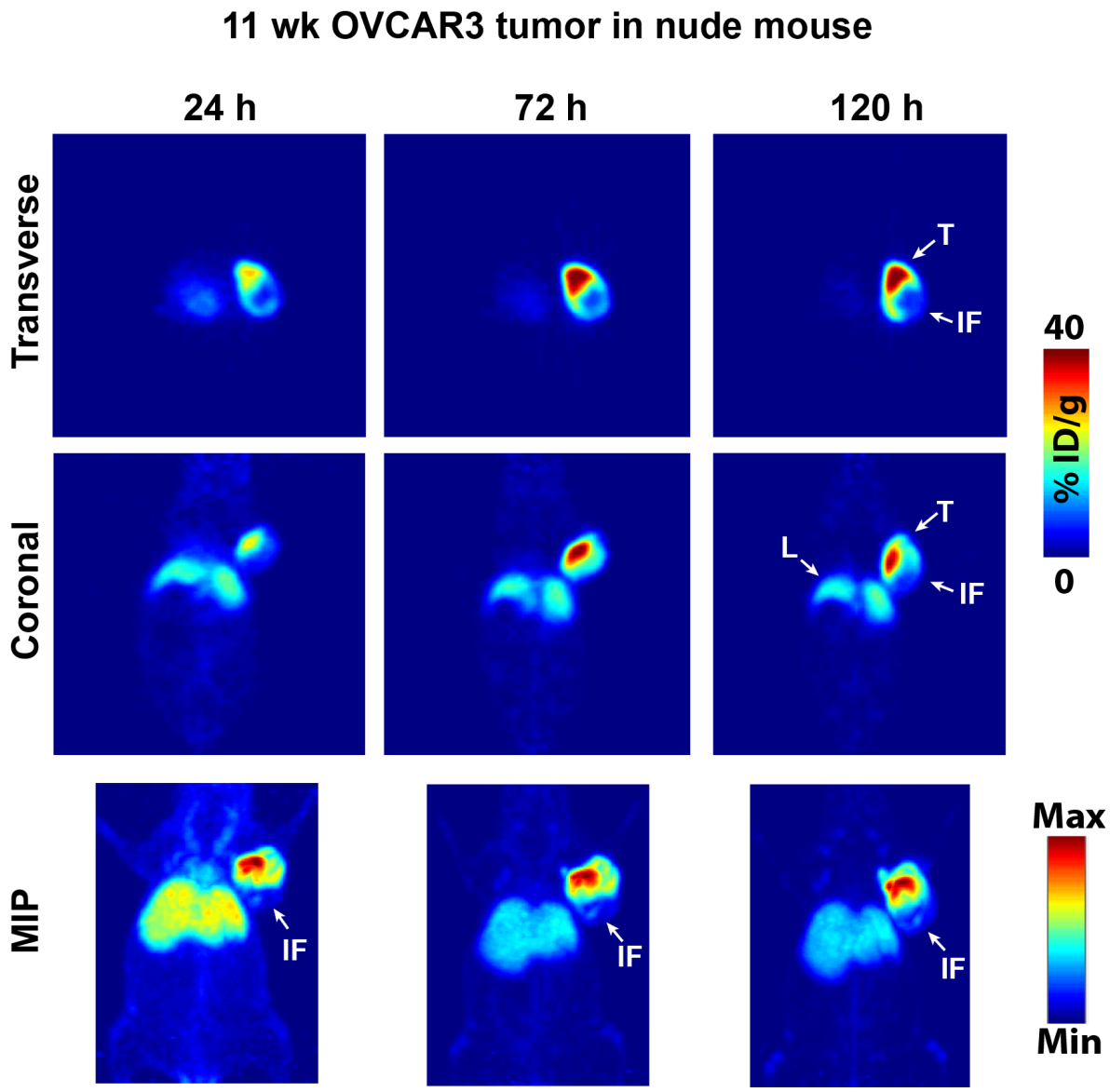


**Supplemental Fig.**
**17. Small Animal PET imaging of OVCAR3 Tumor with $^{89}$Zr-DFO-MAb-B43.13:**

Transverse, Coronal and Maximum Intensity Projection (MIP) serial PET images of $^{89}$Zr-DFO-MAb-B43.13 [10.2 – 12.0 MBq (275-325 μCi) injected via tail vein in 200 μL 0.9 % sterile saline] in athymic nude mouse bearing a 11-week old subcutaneous CA125-positive OVCAR3 xenografts on the right shoulder. The animal had a large cystic tumor. PET imaging was performed at 24, 72 and 120 h post-injection of $^{89}$Zr-DFO-MAb-B43.13. Arrows in the figure indicate the following: tumor (T), interstitial fluid (IF), liver (L), and lymph nodes (LN).

## References


**1.** Sharma SK, Wuest M, Wang M, et al. Immuno-PET of epithelial ovarian cancer: harnessing the potential of CA125 for non-invasive imaging. *EJNMMI Res*. 2014;4:60.

**2.** Lindmo T, Boven E, Cuttitta F, Fedorko J, Bunn PA, Jr. Determination of the immunoreactive fraction of radiolabeled monoclonal antibodies by linear extrapolation to binding at infinite antigen excess. *J Immunol Methods*. 1984;72:77-89.

**3.** Carlin S, Khan N, Ku T, Longo VA, Larson SM, Smith-Jones PM. Molecular targeting of carbonic anhydrase IX in mice with hypoxic HT29 colorectal tumor xenografts. *PLoS One*. 2010;5:e10857.